Impact of narrow-band excitation on resonant decay spectra

E. Pahl, J. Brand, and L. S. Cederbaum
Theoretische Chemie, Physikalisch-Chemisches Institut, INF 229, D-69120 Heidelberg, Germany

F. Tarantelli
Dipartimento di Chimica and Centro Studi CISM-CNR, Università di Perugia, 06123 Perugia, Italy
(Received 22 December 1998)

The influence of narrow-band excitation on the decay spectra of dissociative core-excited molecular states is investigated in detail. Surprising interference phenomena have been reported previously in the resonant Auger spectrum of HF of Pahl *et al.* [Phys. Rev. Lett. **80**, 1865 (1998)]. Apart from a general quenching of the ''atomic'' contribution by detuning, pronounced interference patterns are found for small detuning above the resonance of the core-excited state. Utilizing the time resolution gained within the theory of wave-packet dynamics, the underlying interference mechanisms are analyzed thoroughly. Special attention is paid to the selection process of intermediate-state eigenfunctions accompanying narrow-band excitation. We present a method that enables the assignment of different contributions in the decay spectrum to the internuclear distances at which the corresponding transitions take place. In particular, information about the origin of the atomic transitions is obtained. [S1050-2947(99)00208-5]

PACS number(s): 33.80.Eh, 32.80.Hd, 33.20.−t, 33.70.−w

I. INTRODUCTION

Core-hole molecular states are, in general, short lived and decay on a femtosecond time scale via emission of Auger electrons or x-ray photons. Since the time scale of nuclear dynamics (vibrations or dissociation of the molecule) is of the same order of magnitude as the lifetime of the core-hole state, pronounced interferences can occur and influence strongly the observed Auger or x-ray spectra. Additional interferences are introduced if the initial excitation step is performed in an energetically selective manner. The energy selectivity implies a prolongation of the excitation time, which thus can become comparable to the decay time and the typical time scale of internal motion of the molecule. Such a ''narrow-band'' excitation is very useful if the decay of core-excited states is monitored in the so-called resonant decay spectroscopies because it allows for a selective excitation of only one of the, in general, many and close-lying core-excited states. In the last years, considerable advances have been made in measuring highly resolved resonant Auger [2–5] and x-ray emission [6,7] spectra.

It has been shown that a time-dependent wave-packet picture [8–11] is very well suited for the investigation of such decay processes. Compared with the traditional time-independent picture [12–15] it allows for an additional time-resolved description. The whole information about the creation and decay of core-excited states is contained in the nuclear wave packets of the core-excited and final electronic states. These wave packets are generated by a superposition of earlier created propagating parts and parts added at later times. Their evolution on the potential curves of the corresponding electronic states describes the nuclear dynamics in the respective states.

Interferences can be traced back to this superposition of earlier and later contributions. The appearance of interferences, as well as their constructive or destructive nature, depend on the evolution of the wave packet during its creation and decay, i.e., on the nuclear motion in the corresponding electronic states. A first condition for interferences to occur at all is that the time scales of the creation process and the nuclear dynamics in the populated states are comparable. As mentioned above, the decay spectra of core-hole states can, therefore, be influenced either by interferences occurring in the wave packet of the core-hole state or in the final-state wave packet(s). The condition for the interferences to occur is a comparable time scale of the excitation process and the nuclear dynamics in the core-excited state, or of the decay process and the nuclear dynamics in the final state(s). Another necessary condition for interferences is that already existing and propagating parts of the wave packet remain at least partially localized in the region of their creation during the creation process. This condition is usually fulfilled for bound potential curves, leading to ''vibrational structure:'' in this case, the motion of the wave packet describes the vibration of the molecule and thus remains within the potential well. For dissociative curves, however, the parts of the nuclear wave packet describing the dissociation of the molecule typically leave the zone of their creation very quickly, leading to a suppression of interference.

Nevertheless, also for transitions between purely repulsive curves, pronounced interferences can be found as has been reported recently [1]. Besides a general quenching of the ''atomic'' contributions (originating from the decay after dissociation of the core-excited molecule), one finds very pronounced interferences for small detuning of the excitation energy above the resonance of the core-excited state. In this paper we will illustrate these effects further by giving a detailed analysis based on the wave-packet description. As in Ref. [1] we will concentrate on the realistic example of one specific decay contribution to the resonant Auger spectrum of HF. The corresponding transition yields one of the main contributions to the broad-band resonant Auger spectrum, which has been studied thoroughly in a preceding publication [16]. In that reference, the computed potential curves of

the relevant core-excited and final electronic states have been presented and discussed.

After a short outline of the theory of wave-packet dynamics [8–11], in Sec. II we will review the phenomena introduced by narrow-band excitation (Sec. III). In Sec. IV we start with an investigation of the mechanisms of the selection process in the case of narrow-band excitation (Sec. IV A) before turning to a detailed discussion of the observed effects (Secs. IV B–IV E). Finally, in Sec. IV F we will analyze the different contributions of the decay spectra in relation to the origin of the corresponding transitions. This allows us to answer the question at which internuclear distances ''atomic'' transitions take place.

II. THEORY

In this section we will give a short review of the theory of wave-packet dynamics for the description of the decay of core-hole states. The time-dependent formalism has been developed in the last years for the case of broad-band [8,9] as well as narrow-band excitation [10,11] including the possibility of vibronic coupling either in the manifold of decaying or in the manifold of final states [9,11]. The central point of the theory consists of a set of differential equations that describe the propagation of the nuclear wave packets. These differential equations have been derived by making use of the local approximation, which allows for the derivation of an effective non-Hermitian Hamiltonian of the intermediate state. Within this well-justified approximation the decay is regarded as an irreversible process. In the present context we are interested in the case of an energetically selective excitation (narrow-band case). Within the approximation of a weak electromagnetic field as an exciting source the set of differential equations reads [10]

$$i\dot{\Psi}_d(R,t)=g(t)V\Psi_i(R,t)+\left(\hat{H}_d-\frac{i}{2}\Gamma\right)\Psi_d(R,t), \quad (1)$$

$$i\dot{\Psi}_f(E,R,t)=W\Psi_d(R,t)+(\hat{H}_f+E)\Psi_f(E,R,t). \quad (2)$$

The nuclear wave packets $\Psi_i(R,t)$, $\Psi_d(R,t)$, and $\Psi_f(R,E,t)$ contain the whole information about the nuclear dynamics in the initial, core-excited, and the final electronic states, respectively. Note that $\Psi_f(R,E,t)$ depends not only on the nuclear coordinates R and the propagation time t but also on the energy E of the particle (Auger electron or x-ray photon) emitted during the decay. Since we do not want to calculate angle-resolved decay spectra here, the dependence on the angular quantum numbers has been omitted.

The Hamiltonians of the decaying and final state, $\hat{H}_d$ and $\hat{H}_f$, govern the propagation on the corresponding potential curves. The inhomogeneities $g(t)V\Psi_i(R,t)$ and $W\Psi_d(R,t)$ introduce contributions from the initial to the excited intermediate state and from the latter one to the final state. V and W denote the respective transition matrix elements. Throughout this paper they will be assumed to be independent of the nuclear coordinates R. The function $g(t)$ defines the shape of the excitation pulse. The decay of the core-excited state is accomplished by the imaginary part of the effective Hamiltonian $\hat{H}_d-(i/2)\Gamma$ where Γ denotes the decay width of the core-excited state. The decay width is inversely proportional to the lifetime of this state.

Looking at differential equations (1) and (2) the sources of interferences can easily be identified. Both the intermediate- and final-state wave packet are formed by a superposition of two terms: the already existing part of the wave packet that propagates under the influence of the corresponding potential curves and a source term describing the excited and decaying contributions, respectively. Whenever the time scales of the nuclear dynamics and the process of creation are comparable, interferences can occur. In the case of broad-band excitation this condition of comparable time scales for intermediate-state interferences is not fulfilled because the excitation is very quick in comparison with the nuclear dynamics and can be viewed as an instantaneous process. The excitation function $g(t)$ can thus be well described by a δ function and the source term $g(t)V\Psi_i(R,t)$ in Eq. (1) may be replaced by an initial condition.

All spectroscopically relevant information can be extracted from the wave packets. For example, the intensity $\sigma_f(E,t)$ of the emitted particles as function of their kinetic energy E and the time t can be computed from the final-state wave packets [8]:

$$\sigma_f(E,t)=\int dR|\Psi_f(R,E,t)|^2. \quad (3)$$

The final decay spectrum is obtained for sufficiently large times (in relation to the excitation and decay times):

$$\sigma_f(E)=\lim_{t\to\infty}\sigma_f(E,t). \quad (4)$$

Formula (3) makes obvious the main advantage of the time-dependent over the time-independent formalism: By virtue of the time-resolved information, the formation of the decay spectra can be traced in time. Experimentally, this process could be monitored by pump-probelike experiments with a sudden depopulation of the decaying state.

We want to stress here that the additional time parameter is not necessarily disadvantageous computationally. On the contrary, the time-dependent picture becomes even profitable with increasing size of the problem (e.g., multidimensional systems) because it avoids the diagonalization of large matrices and the storage of large amounts of data typical of time-independent formalisms for the computation of the intensity [2,10]:

$$\sigma_f(E)\propto\sum_{n_f}|M(E+E_{n_f})|^2\left|\sum_{n_d}\frac{\langle n_f|n_d\rangle\langle n_d|\Psi_i\rangle}{E-(E_{n_d}-E_{n_f})+i\Gamma/2}\right|^2. \quad (5)$$

Here, for the evaluation of $\sigma_f(E)$, the Hamiltonians $\hat{H}_d$ and $\hat{H}_f$ have to be diagonalized and all the eigenvectors $|n_d\rangle$ and $|n_f\rangle$ and eigenvalues E_{n_d} and E_{n_f} have to be stored. $M(\omega)$ denotes the Fourier transform of the excitation function $g(t)$.

In addition to $\sigma_f(E)$, the total integrated intensity Ω represents another important spectroscopic quantity in the case of narrow-band excitation, because it measures the extent of radiation, which is absorbed during the excitation process.

The maxima of Ω as a function of the excitation energy define the resonances of the intermediate states. In Ref. [10] the following formula has been derived:

$$\Omega = \sum_{n_d} |\langle n_d|V|\Psi_i\rangle|^2 G(E_{n_d}), \tag{6}$$

with

$$G(E_{n_d}) = \int_{-\infty}^{\infty} d\omega \frac{\Gamma/2\pi}{(E_{n_d}-\omega)^2+(\Gamma/2)^2}|M(\omega)|^2.$$

On the basis of formula (6) one can easily see that the total integrated intensity depends strongly on the Franck-Condon overlaps between the initial and intermediate electronic states. If the level spacing in the intermediate state is much smaller than both the energy width of the excitation function $M(\omega)$ and the decay width Γ, $G(E_{n_d})$ follows the shape of the excitation function. This, of course, is always the case for dissociative states. Integration of $G(E_{n_d})$ over the energies E_{n_d} weighted with the Franck-Condon overlaps then yields the total integrated intensity Ω. The resonance of a dissociative state thus coincides roughly with the maximum of the Franck-Condon overlaps.

The numerical procedure to compute the partial Auger intensities $\sigma_f(E)$ either within the time-dependent or within the time-independent framework according to Eqs. (3) and (4), or Eq. (5), respectively, has been described in detail in Ref. [10]. Here, we only want to mention briefly that we use a uniformly spaced grid on which the wave functions Ψ_d and Ψ_f are represented and propagated. The time propagation is performed by using a short-iterative Lanczos integrator [17–19]; the kinetic energy is applied via fast-Fourier-transform. In implementing the time-independent formula we represent the Hamiltonians $\hat{H}_d$ and $\hat{H}_f$ by a discrete-variable-representation (DVR) variant [20] and compute the needed eigenvectors $|n_d\rangle$ and $|n_f\rangle$ as well as the eigenvalues E_{n_d} and E_{n_f} by diagonalization.

III. RESULTS

In order to demonstrate and analyze in detail the effects introduced by detuning in the case of dissociative states we will concentrate on the particular Auger transition from the lowest-lying core-excited state of HF into the repulsive final state $HF^+(^4\Pi: \ldots 3\sigma^1 1\pi^3 4\sigma^1)$ dissociating into F^+ and H:

$$\begin{array}{ccc} HF(^1\Sigma^+) & \rightarrow HF^*(^1\Sigma^+) & \rightarrow F^*(^2S)+H(^2S) \\ & \downarrow \qquad\qquad \downarrow & \\ & HF^+(^4\Pi) \rightarrow F^+(^1D)+H(^2S). & \end{array}$$

From the electronic and vibrational ground state ($\Psi_i = |n_i\rangle$) of HF, the intermediate state $HF^*(^1\Sigma^+)$ is populated by narrow-band excitation. Since the core electron is excited into the antibonding 4σ molecular orbital, the intermediate state exhibits a strongly repulsive character. Due to the repulsive character of both the intermediate and final state, one finds, apart from the competition of excitation and decay, an additional interplay between the ''molecular'' Auger decay and the decay of the core-excited F* atom. The decay transition we are considering yields one of the main contributions to the full resonant Auger spectrum [16], which we have calculated based on *ab initio* correlated quantum-chemical computations of the lowest-lying potential curves of the core-excited state and of the final cationic states. Details of these computations as well as an analysis of the experimental electron energy-loss spectrum [21] and the broad-band resonant Auger spectrum [22] are given in Ref. [16].

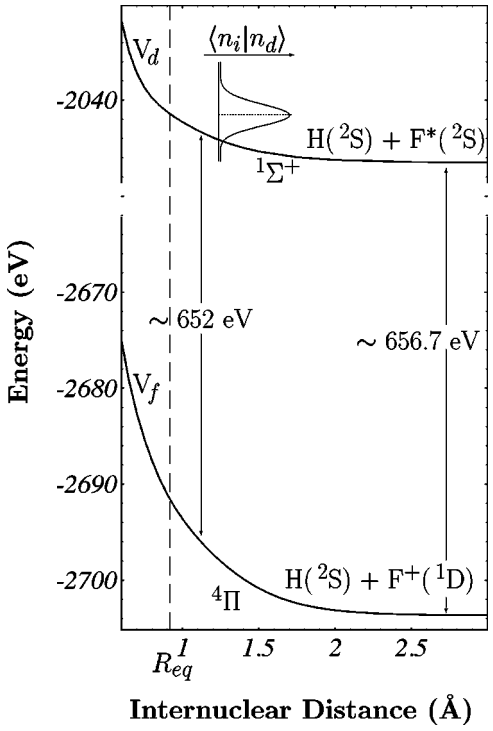

FIG. 1. *Ab initio* potential curves of the core-excited $^1\Sigma^+$ state dissociating into $H(^2S)+F(^2S)$ and the cationic $^4\Pi$ final state, which dissociates into $H+F^+(^1D)$. Additionally, the Franck-Condon overlaps between the initial-state wave function $|n_i\rangle$ and the eigenvectors of the intermediate state $|n_d\rangle$ are depicted. The resonance of the $^1\Sigma^+$ state coincides roughly with the maximum of the Franck-Condon overlaps as indicated by the dashed line. The arrows show the region of the ''molecular'' and ''atomic'' transitions leading to contributions to the resonant Auger spectrum at about 652 eV and at 656.7 eV, respectively. The dashed line indicates the equilibrium distance $R_{eq}=0.92$ Å of HF.

In Fig. 1 we display the potential curves of the $^1\Sigma^+$ core-excited and the $^4\Pi$ final state involved in the transition under study. Figure 2 shows the corresponding contribution to the broad-band Auger spectrum. We see here a pronounced two-peak structure, typical of a transition between two purely dissociative curves. The sharp atomic peak appears at 656.7 eV, corresponding to the energy difference between the dissociation limits of the intermediate- and final-state potential curves. The molecular tail is found at lower energies at about 652 eV.

The study of this transition serves as a model example for the interference effects appearing in the case of dissociative curves. Apart from the nature of the potential curves involved, these effects depend only on details of the excitation process. Similar effects are always to be expected when the energy width of the incoming radiation becomes of the same

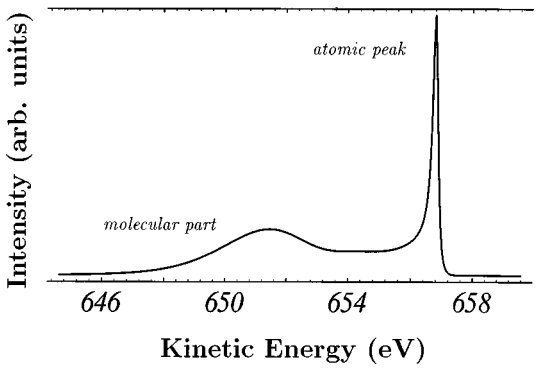

FIG. 2. Contribution to the broad-band Auger spectrum of HF resulting from the transition between the core-excited $^1\Sigma^+$ state and the cationic $^4\Pi$ final state. One can identify very well the typical two-peak structure formed by the intense and sharp ''atomic'' peak at 656.7 eV and the broad ''molecular'' part at about 652 eV.

order of magnitude as the decay width of the core-excited state. Throughout this paper we have chosen an excitation width [full width at half maximum (FWHM)] of 0.2 eV. The excitation pulse is centered at the zero of the time scale. Due to the selection of a Gaussian-shaped excitation function the chosen excitation width corresponds to a pulse duration of 13 fs. The decay width of the core-excited state is also taken as 0.2 eV. This value corresponds to the decay width of core-ionized HF^+, which has been determined experimentally [23] as well as theoretically [24]. From the experimental electron energy-loss spectrum [21], the same value for the decay width has also been estimated for the core-excited $^1\Sigma^+$ state considered here, corresponding to a lifetime of 9 fs.

The investigation of the decay of the core-excited $^1\Sigma^+$ state of HF is particularly well suited for the study of the effects of detuning because this state is very well separated (by about 4 eV) from the higher-lying core-excited Rydberg states [16]. In the case of the experimentally well-studied resonant Auger decay of HCl [25,5], for example, the lowest-lying $2p_{3/2}^{-1}4s$ resonance is separated only by about 1 eV from the corresponding $2p_{1/2}$ resonance, and the latter state only 1.5 eV from the first Rydberg state. This implies a severe limitation when detuning towards higher excitation energies.

The resonance of the $^1\Sigma^+$ core-excited state, which is defined as the maximum in the total integrated intensity Ω, lies at an excitation energy of about 687 eV. In correspondence with Eq. (6), the resonance coincides roughly with the maximum of the Franck-Condon overlaps $\langle n_i|n_d\rangle$ but is slightly shifted towards higher energies due to an asymmetry in the Franck-Condon distribution (see the inset in Fig. 1). Let us now consider Fig. 3. At the top we have depicted the narrow-band spectrum of the transition taken at the resonance energy defined above. Below, several off-resonance spectra are displayed. In the left and right columns the excitation energy is detuned below and above the resonance, respectively, by an amount increasing from top to bottom. While the on-resonance spectrum resembles closely the corresponding broad-band spectrum (Fig. 2), one observes significant changes when detuning the excitation energy. Apart from the expected loss in the total integrated intensity Ω, we find the following:

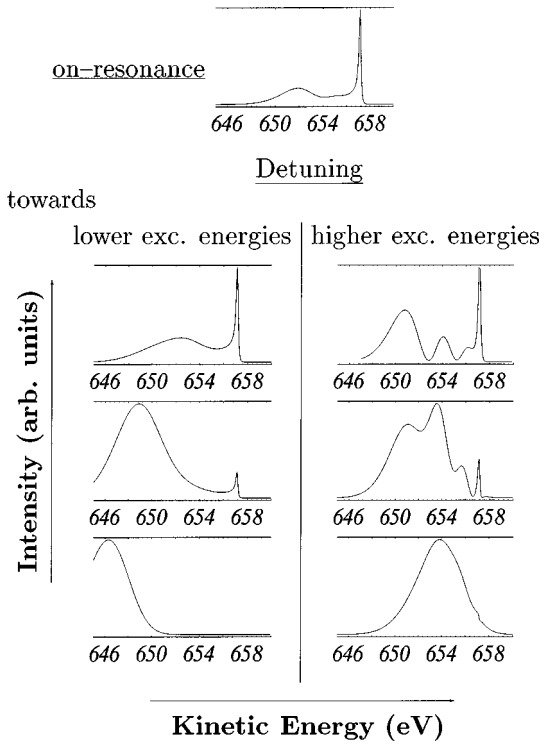

FIG. 3. Contribution to the narrow-band Auger spectrum of HF resulting from the transition between the core-excited $^1\Sigma^+$ state and the cationic $^4\Pi$ final state for different excitation energies E_{exc}. The excitation width is 0.2 eV (FWHM). At the top the on-resonance spectrum ($E_{exc}=687$ eV) is shown. Displayed below, on the left and right sides, are the off-resonance spectra resulting from detuning towards lower and higher excitation energies, respectively. The excitation energies from top to bottom are $E_{exc}=685$ eV, 684 eV, and 682 eV on the left, and $E_{exc}=689$ eV, 690 eV, and 691 eV on the right. The total integrated intensity Ω decreases strongly by detuning. Having set to $\Omega=1$ for the broad-band spectrum of Fig. 1, we find $\Omega=0.357$ on resonance. For the detuned spectra on the left we find from top to bottom: $\Omega=0.04$, 0.005, and 0.001; for the detuned spectra on the right from top to bottom: $\Omega=0.016$, 0.03, and 0.002.

(i) For small detuning towards higher excitation energies (right-hand side of Fig. 3), a very pronounced structure appears in the molecular part of the spectrum. At first glance, this is very astonishing because we are concerned with a transition between purely dissociative curves, where interference effects are strongly suppressed, in general.

(ii) For large detuning only the broad molecular part of the spectrum remains, showing a linear dispersion with the excitation energy. The energy width (FWHM) of the peak is about 4 eV and is, over a wide range, independent of the excitation width (see also Fig. 10).

(iii) The relative intensity of the atomic peak with respect to the molecular part decreases by detuning, also for detuning towards higher excitation energies. This quenching of the atomic line has been predicted before [10] and hints for this phenomenon have been found later in the study of the resonant Auger spectrum of HCl [25].

IV. DISCUSSION OF THE RESULTS

In the following we will discuss the observed effects after focusing on the mechanisms of the selection process caused by narrow-band excitation. These mechanisms turn out to be crucial for the understanding of the observed effects.

A. The selection process in the narrow-band case

In the case of an energetically unselective (broad-band) excitation, the excitation process is very quick in comparison with the decay. The excitation can in fact be viewed as an instantaneous event in which the initial-state wave packet is transferred vertically to the potential curve of the intermediate electronic state. Consequently, no interferences in the intermediate-state wave packet are found. An energetically selective (narrow-band) excitation, on the other hand, leads to a prolongation of the excitation time. The intermediate-state wave packet $\Psi_d(R,t)$ is now formed by a superposition of contributions added continuously during the excitation. Interferences take place between the earlier and later created parts, and guarantee the desired energy selection.

In order to illuminate this selection process further it is useful to decompose the intermediate-state wave function $\Psi_d(R,t)$ into the eigenvectors $|n_d\rangle$ of the intermediate electronic state and to look at the squared absolute values of the overlaps $|\langle n_d|\Psi_d(t)\rangle|^2$ as a function of the corresponding eigenvalues E_{n_d}. In Fig. 4 the time evolution of these overlaps for the present case is shown for three values of the excitation energy: below the resonance ($E_{exc}=685$ eV) in column (a), at the resonance ($E_{exc}=687$ eV) in column (b), and above the resonance ($E_{exc}=689$ eV) in column (c). For the sake of comparison, the squared absolute value of the Franck-Condon overlaps between the initial-state wave function $|n_i\rangle$ and the eigenvectors $|n_d\rangle$ are additionally shown in each frame by the dashed lines. This Franck-Condon distribution corresponds to the population of the intermediate-state levels in the case of broad-band excitation. In that case, the shape of the distribution does not change in time; only the magnitude of the overlaps decreases exponentially as $e^{-\Gamma t}$, where Γ is the decay width of the intermediate state.

In Fig. 4 one can see very well that in the narrow-band case the population of the intermediate-state levels at the very beginning of the excitation process are heavily influenced by the Franck-Condon overlaps but traces of the energy selection of the excitation pulse can already be found. With some time delay, the selection works more and more efficiently by interference between earlier and later created parts of $\Psi_d(R,t)$. The selection process works by filtering out those levels that lie in the desired energy region, corresponding to the width of the excitation. For on-resonance excitation the ''correct'' levels are populated already from the beginning and the interferences are thus of a mainly constructive character. With increased detuning below or above the resonance, however, the interferences become more and more destructive and the ''wrongly'' excited components of the wave packet are destroyed in time. Note again that the resonance energy is defined as the maximum of the total integrated intensity Ω of Eq. (6). Due to the asymmetric shape of the Franck-Condon overlaps this resonance does not coincide exactly with the maximum of the Franck-Condon distribution but is shifted to slightly higher energies.

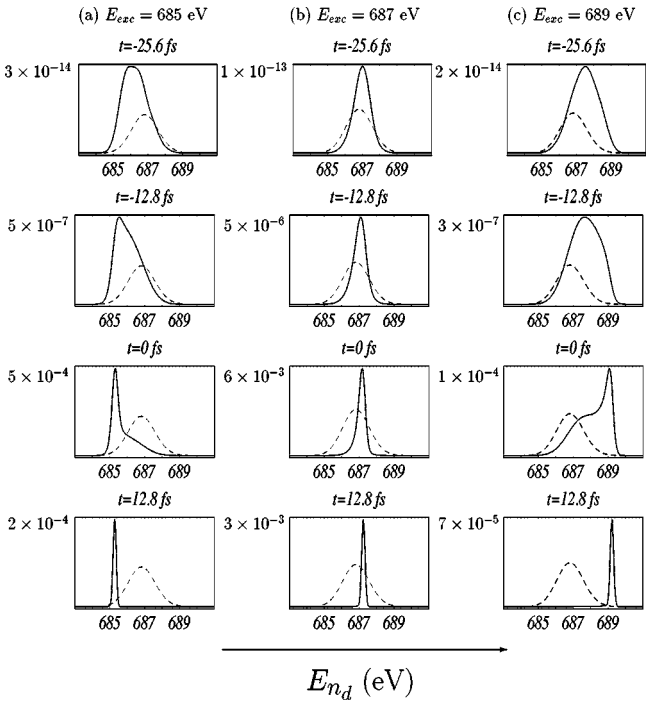

FIG. 4. The solid-line plots show the time evolution of the square magnitude $|\langle\Psi_d(t)|n_d\rangle|^2$ of the overlap between the intermediate-state wave packet and the ''eigenvectors'' of the intermediate state as a function of the corresponding energies E_{n_d}: (a) for below-resonance excitation ($E_{exc}=685$ eV), (b) for the on-resonance case ($E_{exc}=687$ eV), and (c) for an excitation above the resonance at $E_{exc}=689$ eV. Note the change in ordinate scale in the different frames. The dashed-line plots show the corresponding squared Franck-Condon overlaps $|\langle n_i|n_d\rangle|^2$ adjusted to the corresponding ordinate scales. At the beginning of the excitation process the population distribution of the intermediate state roughly matches these overlaps. Then, with some time delay, the desired energy selection is achieved by (constructive and destructive) interference.

According to the changing interference patterns depending on the extent of detuning one can observe a different behavior in the intermediate-state population. In Fig. 5 the time evolution of the squared norm of the intermediate-state wave packet $\int dR|\Psi_d(R,t)|^2$ is displayed on a logarithmic scale for broad-band excitation as well as for narrow-band excitation at several excitation energies. In the broad-band case the intermediate-state wave packet is created instantaneously at time $t=0$ by transferring the normalized initial-state wave packet to the intermediate state. For $t>0$ the wave packet decays exponentially. In the narrow-band case constructive interferences prevail for on-resonance excitation and the norm grows until the exponential decay becomes the dominant process. In the figure, this onset of exponential decay is indicated by the transition to the linear decrease. Below and above the resonance, the wave packet initially created on the intermediate state is increasingly destroyed by interferences for $t>0$ but still during the excitation process. The stronger the detuning the more closely the norm of the wave packet follows the excitation pulse. The maximum of the norm shifts from positive times to $t=0$, which corresponds to the center of the excitation pulse. The resulting decay spectra are thus increasingly dominated by the short-

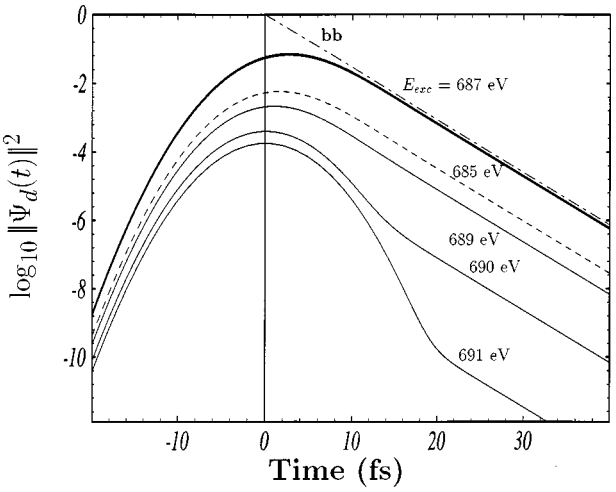

FIG. 5. Time evolution of the norm of the intermediate-state wave packet $\Psi_d(t)$ for broad-band excitation and at various narrow-band (0.2-eV FWHM pulse) excitation energies. The squared norm is plotted on a logarithmic scale and the onset of the exponential decay can, therefore, be identified by the transition to the linear decrease. The dashed-pointed line describes $\int dR|\Psi_d(t)|^2$ in the broad-band (depicted as **bb**) case in which the intermediate-state wave packet is created instantly at $t=0$. The thick line shows the behavior in the on-resonance case ($E_{exc}=687$ eV). The dashed line corresponds to below-resonance excitation, the thin lines correspond to above-resonance excitation. The excitation energies are chosen as indicated in the plot.

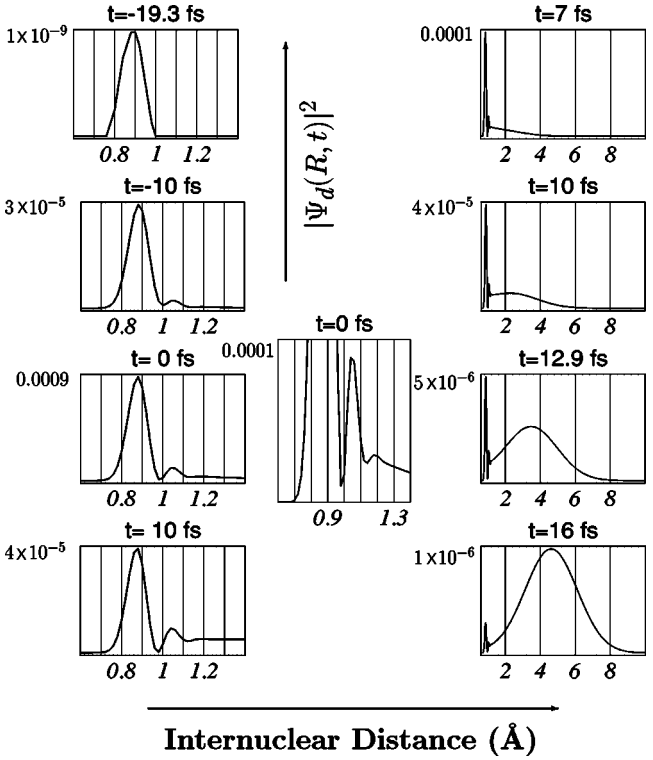

FIG. 6. Time evolution of the intermediate-state spatial distribution $|\Psi_d(R,t)|^2$ for small detuning towards higher excitation energies ($E_{exc}=689$ eV). The width of the excitation is 0.2 eV (FWHM). Note the change in ordinate scale for the different frames. On the left-hand side the short-time behavior is shown for small, ''molecular,'' internuclear distances. In the center an additional magnified frame shows the three-peak structure at $t=0$ (the center of the excitation pulse). On the right-hand side the long-time behavior is depicted for a wider range of internuclear distances. One can see that the dissociation of the intermediate state occurs relatively slowly in comparison with the formation of the structure, which itself is connected with the duration of the excitation.

time behavior and the observed contributions correspond less and less to transitions from the levels actually selected by the pulse. For strong detuning one can finally describe the resulting spectra very well within the concept of a *decrease of the effective lifetime* [10,26]. The consequences for the decay spectra will be discussed in detail in Sec. IV D.

Concluding, we have seen that for narrow-band excitation an energy selection is only efficient at the resonance and for small detuning away from the resonance. Because of the decrease of the effective lifetime and the onset of Raman-like behavior with detuning, the norm of the intermediate-state wave packet becomes negligible before energy selection can take place. This fact suppresses the possibility of an energy-selective spectroscopy by using off-resonance excitation. This suppression becomes stronger the more the pulse leaves the energy region accessible by broad-band excitation [i.e., the Franck-Condon ($\langle n_i|n_d\rangle$) region].

B. Small detuning above the resonance

For a small detuning towards higher excitation energies one finds a very pronounced structure in the resulting Auger spectra, as we can see on the right-hand side of Fig. 3. At an excitation energy of 689 eV, which means 2 eV above the resonance, three well-defined peaks can be distinguished in the molecular region of the spectrum. This is a very astonishing effect because we are concerned with a transition between purely repulsive potential curves where usually interference effects are strongly suppressed.

The explanation of this effect is connected with the selection process described in the previous section. There, we have seen that only in the vicinity of the resonance the selection works efficiently. For small detuning above the resonance, not only the desired energy is selected by interference but also the nodal structure of the (improper) eigenvectors $|n_d\rangle$ in the selected energy region is transferred to the intermediate-state wave function $\Psi_d(R,t)$. The formation of this structure in $\Psi_d(R,t)$ can be seen in Fig. 6 and will be discussed below. Provided that this structure is sufficiently long-lived, it is then mapped onto the Auger spectrum. Because of the dissociative character of the final-state potential this mapping is particularly simple [26]: Transitions occurring at smaller internuclear distances lead to contributions at lower energies than the transitions at larger distances (see Sec. IV F for a more thorough analysis of this mapping effect).

1. Formation of the structure in the intermediate state

The central questions that we want to address are the following: Why do pronounced interferences occur in the intermediate-state wave packet even though the potential is of a repulsive nature? Why do these interferences arise only for detuning towards higher excitation energies and not on or below the resonance? As an essential condition for interferences we have already mentioned that at least two different time scales involved in the process under study need to be

comparable. For interferences in the intermediate state this requirement refers to the time scales of excitation and nuclear dynamics in the intermediate state. In the examples presented here (Fig. 3) this condition of comparable time scales is always fulfilled because we have chosen the excitation width (inverse of the pulse duration) to coincide with the decay width of the intermediate state ($\mathrm{FWHM}_{exc}=\Gamma=0.2$ eV). Of course, this condition of comparable time scales does not discriminate among excitation on-resonance, above, or below it. Another crucial condition for interferences concerns the spatial localization of the intermediate-state wave packet: parts of the wave packet created earlier in time have to remain localized in the region of their creation, where new parts are added continuously at later times during the excitation process, so that interferences can occur. If one excites at or below the resonance, the wave packet is created near the potential well and is exposed instantly to the repulsive forces of the intermediate-state potential. Consequently, it moves out of the interaction zone very quickly and interferences are suppressed. The intermediate-state wave function $\Psi_d(R,t)$ then describes direct dissociation of the core-excited molecule. With increased excitation energy, i.e., detuning above resonance, parts of $\Psi_d(R,t)$ can now also move in the opposite direction towards smaller internuclear distances. Additionally, the interaction zone is enlarged due to the fact that for higher excitation energies the accessible range of internuclear distances increases. Summing it up, we can state that by detuning towards higher excitation energies, parts of $\Psi_d(t)$ stay longer in an enlarged interaction zone, allowing the formation of a pronounced nodal structure by interference.

The above explanation is confirmed by Fig. 7 where the momentum distribution of the intermediate-state wave function $\tilde{\Psi}_d(P,t)$ is shown as a function of the linear momentum P of the intramolecular motion for different propagation times t. The function $\tilde{\Psi}_d(P,t)$ is obtained by Fourier transformation of the spatial wave function $\Psi_d(R,t)$. On the left-hand side of the figure, $|\tilde{\Psi}_d(P,t)|^2$ is displayed for excitation at the resonance and on the right-hand side, for excitation above (solid line) and below (dashed line) the resonance. Here we will only compare the on-resonance with the above-resonance case; in Sec. IV C we will discuss the behavior for excitation below the resonance.

At the very beginning of the excitation one finds a similar momentum distribution both on-resonance and above. The center of the distribution is shifted slightly towards positive momenta. While the initial peak in the momentum distribution remains stationary during the whole excitation process for the off-resonance excitation, almost only positive momenta are found after a very short time in the on-resonance case. This reflects the fact that the wave packet describes an immediate dissociation of the molecule in the on-resonance case. At higher excitation energies, on the other hand, parts of the intermediate-state wave packet carry very little or even negative momentum and thus remain in the interaction region, with only a small tail describing immediate dissociation. At about $t=0$, a sharp peak begins to develop in the momentum distribution at positive momenta. This peak corresponds to the outward movement of the HF molecule in the dissociation limit and thus can be ascribed to the atomic peak

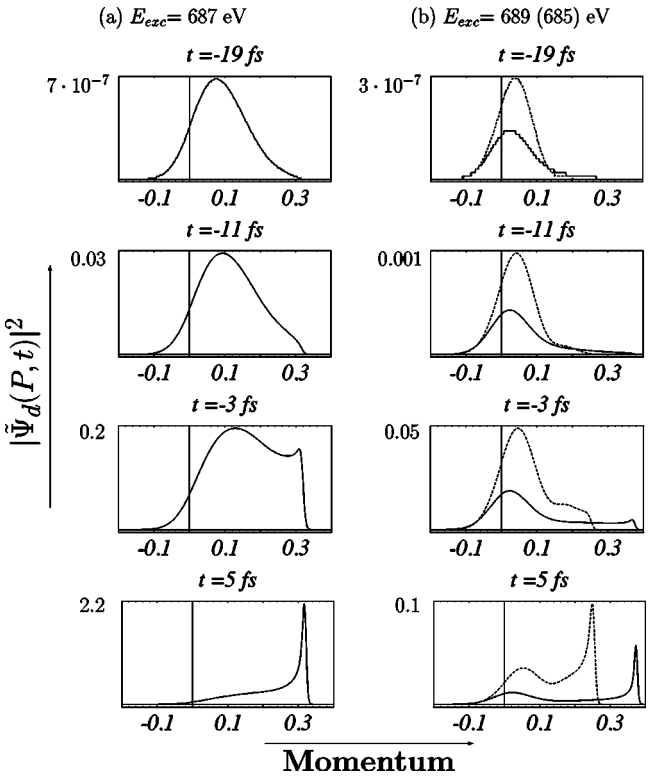

FIG. 7. Time evolution of the momentum distribution $|\tilde{\Psi}_d(P,t)|^2$ of the intermediate-state wave packet (a) for on-resonance excitation; (b) above (solid line) and below (dashed line) the resonance. The width of the Gaussian excitation pulse is chosen to be 0.2 eV, while its center defines the zero of the time scale. The momenta are displayed in units of μ_{HF} Å/fs where $\mu_{\mathrm{HF}}=1.59\times10^{-27}$ kg denotes the reduced mass of HF. Note that the ordinate scale changes in the various frames.

in the spectrum. Due to the higher excitation energy the ''atomic peak of the momentum distribution'' is found at higher momenta for the above-resonance excitation than for the on-resonance excitation.

According to this explanation, the appearance of the structure in $\Psi_d(t)$ should mainly depend on the strength of the detuning above the resonance and not on the gradient of the intermediate-state potential curve. This statement can be proven by artificially shifting the potential curve of the initial state horizontally against that of the intermediate state: Figure 8 shows spectra obtained with a hypothetical equilibrium distance of $R_{eq}=0.8$ Å (instead of the real distance of $R_{eq}=0.92$ Å). The equilibrium distance is chosen such that the ''new'' resonance is now found at an excitation energy of $E_{exc}=689$ eV, where before the interference structure had been observed. Now, this structure is suppressed [Fig. 8(a)] for on-resonance excitation. Increasing the excitation energy by 2 eV, the structure reappears [Fig. 8(b)]. The generally broader molecular features of the spectra of Fig. 8 in comparison with Fig. 3 can be explained by the steeper gradient of the intermediate-state potential curve in the (now translated) region of excitation.

2. Time evolution of the spectrum

Figure 9 shows the time evolution of the spectrum taken at an excitation energy of $E_{exc}=689$ eV. Due to the ''map-

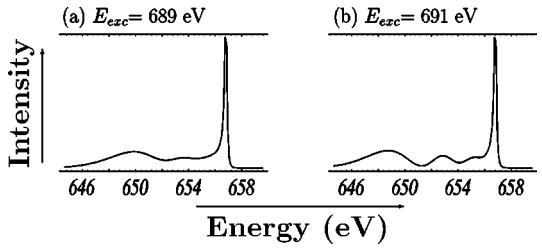

FIG. 8. Narrow-band Auger spectra for the transition between the core-excited $^1\Sigma^+$ state and the cationic $^4\Pi$ final state occurring upon excitation from an initial state shifted horizontally against the intermediate state. The equilibrium distance R_{eq} of the ground state is artificially reduced from 0.92 Å to 0.8 Å. Therefore, the resonance is now found at an excitation energy of $E_{exc}=689$ eV. Part (a) shows the spectrum taken at the ''new'' resonance, which now does not exhibit a pronounced structure. (b) By detuning 2 eV above the resonance ($E_{exc}=691$ eV) the structure appears again. The total integrated intensity is (a) $\Omega=0.21$ and (b) $\Omega=0.04$.

ping'' effect of the dissociative final-state potential curve, the time evolution of the spectrum is closely related to the evolution of the intermediate-state wave packet shown in Fig. 6. At the very beginning of the excitation, the spectrum reflects the Gaussian shape of the initial-state wave function. The spectrum is dominated by molecular contributions about 651 eV, coming from vertical transitions, which take place about the equilibrium position ($R_{eq}=0.92$ Å) of the ground state. At later times also transitions at larger internuclear distances and thus contributions at higher Auger energies occur, due to the outgoing parts of the intermediate-state wave packet. With some time delay the interference structure is generated in accordance with the energy selection taking place. The two additional peaks at about 654 and 656.2 eV are formed successively. As we will see in Sec. IV F these peaks can be assigned to transitions occurring at internuclear distances of 1–1.5 Å and 1.5–2.5 Å, respectively. After the molecular part of the spectrum and its interference structure is almost completely formed, at approximately the middle of the excitation pulse ($t=0$), the atomic peak at 656.7 eV begins to arise.

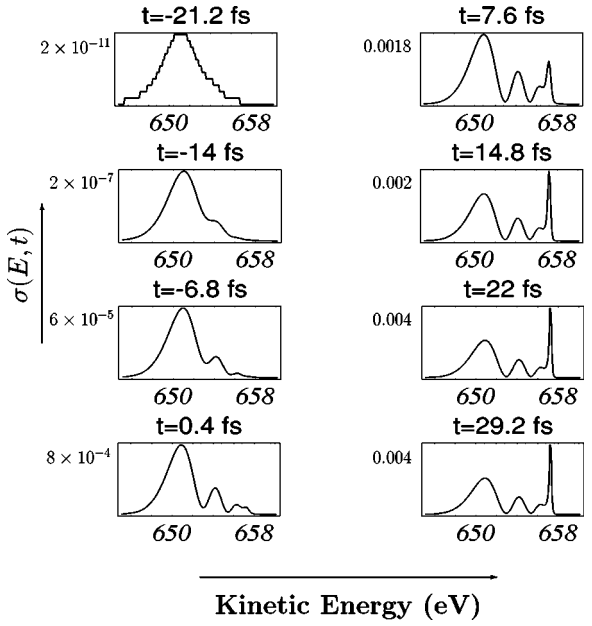

FIG. 9. Time evolution of the Auger spectrum $\sigma_f(E,t)$ for an excitation energy of $E_{exc}=689$ eV, i.e., for small detuning (2 eV) towards higher excitation energies. The excitation width is 0.2 eV. The maximum of the excitation pulse defines the zero of the time scale. Note that the ordinate scale changes in the different frames.

C. Small detuning below the resonance

In Fig. 3 the spectra, which result when detuning towards lower excitation energies, are shown on the left-hand side. For small detuning (see the spectrum at an excitation energy of $E_{exc}=685$ eV) one notes that the molecular part becomes broader compared to that in the on-resonance spectrum. Thus, the whole spectrum resembles now more the broadband spectrum of Fig. 2. This is understandable from the discussion in Sec. IV A, where we have shown that the short-time and thus energetically still unselected contributions, become more important when detuning from the resonance. As explained in Sec. IV B 1 no interference structure shapes the molecular part because the energetically correct and ''surviving'' parts of the intermediate-state wave packet move directly out of the interaction zone and do not interact with later contributions. The larger amount of the outgoing wave packet can also be identified in the momentum distribution $|\tilde{\Psi}_d(P,t)|^2$ [in Fig. 7(b), dashed lines] that shows a significant dominance of positive momenta already from the beginning compared to the above-resonance case. The center of the ''stationary'' peak in the momentum distribution is shifted towards higher momenta yet from the very beginning.

Looking at the time evolution of the norm of the intermediate-state wave packet in Fig. 5, we see that the norm is larger when detuning the excitation energy by the same amount towards lower than towards higher energies. The explanation for this phenomenon lies in the asymmetric shape of the Franck-Condon distribution, which reflects the fact that intermediate-state levels lying below the resonance are preferably populated (see Fig. 4). As a consequence, also the total integrated intensity Ω [see Eq. (6)] is larger below than above the resonance (the total integrated intensity is, e.g., $\Omega=0.04$ for $E_{exc}=685$ eV and $\Omega=0.016$ eV for $E_{exc}=689$ eV).

D. Large detuning of the excitation energy

The spectra obtained for large detuning of the excitation energy off the resonance (at the bottom of Fig. 3) can be understood very well through the concept of an effective lifetime decrease (see Sec. IV A). For strong detuning the decrease of the effective lifetime is considerable and the spectra are dominated by a true short-time behavior, i.e., the spectrum is exclusively formed by vertical molecular transitions, which take place at about the equilibrium position $R_{eq}=0.92$ Å of the ground state. The shape of the final spectrum thus resembles that of the spectrum of Fig. 9 at the very beginning of the excitation pulse (at about $t=-20$ fs). The mean energy of the strongly detuned Auger spectra becomes independent of the energy of the intermediate state and depends only on the energy difference between the excitation energy and the final-state energies [10]. As a consequence of energy conservation the peak shows a linear dispersion with the excitation energy and information about the

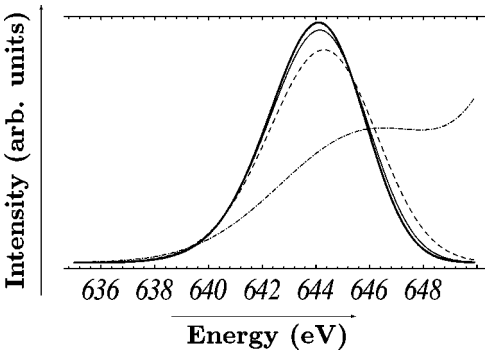

FIG. 10. Molecular part of the Auger contribution of the transition between the core-excited $^1\Sigma^+$ state and the cationic $^4\Pi$ final state for different excitation widths and for large low-energy detuning ($E_{exc}=680$ eV). The excitation widths are 0.1 eV and 0.2 eV (thick line), 1 eV (thin line), 2 eV (dashed line), and 5 eV (dashed-dotted line). One observes that the spectral width follows the excitation width only for very large widths. At an excitation width of 5 eV the excitation is broad enough so that intermediate-state levels favored by the Franck-Condon overlaps $\langle n_i|n_d\rangle$ are populated again and thus also the resonant components arise in the spectrum. The frame is, however, chosen such that this part of the spectrum is skipped.

intermediate core-excited state is lost. This is one of the characteristics of the so-called Auger resonant Raman effect (ARRE) that has been found in atomic (see e.g., [27,28]) as well as in molecular [29,4,30] Auger transitions.

One of the interesting findings in atomic ARRE is that the Auger spectrum narrows with decreasing width of the excitation pulse [27]. We have examined this ''Auger-Raman narrowing'' also in the molecular case. The observed behavior of the spectra under variation of the excitation width (see Fig. 10) is surprising at first sight: The width of the molecular peak remains unchanged under variation of the excitation width in a very wide range of the latter. Only for large excitation widths of about 5 eV one finds a broadening of the molecular peak. This behavior results from the Franck-Condon overlaps between the initial state $|n_i\rangle$ and the eigenvectors $|n_f\rangle$ of the final state, which show a relatively large energy width of about 6 eV due to the dissociative nature of the final-state potential curve. The width of the molecular contribution in the Auger spectrum is determined by the larger of the two widths of the Franck-Condon overlaps and of the excitation function. This means that the additional width introduced by the nuclear dynamics can cover the ''Auger-Raman narrowing'' in the molecular case. This can be easily seen from Eq. (5), considering that for large detuning the denominators become increasingly independent of E_{n_d}. The sum $\Sigma_{n_d}|n_d\rangle\langle n_d|$ can thus be approximately replaced by unity and we find that the energy dependence of the Auger intensity $\sigma_f(E)$ is now governed by products of the excitation function $M(E+E_{n_f})$ and the mentioned Franck-Condon overlaps $\langle n_i|n_f\rangle$.

In order to observe the above-described effects experimentally, detuning towards lower excitation energies is usually necessary in order to avoid the population of neighboring electronic states. Nevertheless, the experimental observation is probably very difficult because of the strong decrease in the total integrated intensity Ω with detuning, as discussed in Sec. IV A. Since Ω is small, direct photoionization could additionally become a competitive (and possibly interfering) channel and should be considered.

E. Quenching of the atomic peak by detuning

The suppression of the atomic peak has already been discussed in detail in Ref. [10]. The atomic peak is built up by transitions occurring after the dissociation of the molecule and is thus a late-time contribution to the spectrum (see also Fig. 6 and Fig. 9). The quenching of the atomic peak by detuning is, therefore, an obvious consequence of the decrease of the effective intermediate-state lifetime introduced by the detuning as described above (see also Fig. 5).

F. The origin of the different contributions

Finally, we present a method that allows for an analysis of the origin of different contributions to the spectrum in relation to the internuclear distance at which they originate and in terms of interferences between different spatial regions. In particular, this method enables us to answer the question of the internuclear distances at which atomic transitions take place. Also, a thorough analysis of the described ''mapping'' effect will be possible.

First, we divide the whole position space into different spatial regions $\mathcal{R}$ (see Fig. 11) and define ''spatially resolved'' partial intensities $\sigma_f^{\mathcal{R}}(E)$. These partial intensities are formed from those contributions originating only from decay in the corresponding spatial region $\mathcal{R}$. In order to compute these quantities, we introduce partial final-state wave packets $\Psi_f^{\mathcal{R}}(E,R,t)$ that are built by transitions in the region $\mathcal{R}$ only. Besides a change in the inhomogeneity $\hat{W}\Psi_d(R,t)$, which is put to zero outside the region $\mathcal{R}$, we propagate these wave functions as usual, i.e., by using the set of differential equations (1) and (2). The partial intensities $\sigma_f^{\mathcal{R}}(E)$ are then obtained in analogy to the total intensity $\sigma_f(E)$ [Eq. (4)] as the time limit of the norm of the partial final-state wave functions:

$$\sigma_f^{\mathcal{R}}(E)=\lim_{t\to\infty}\int dR|\Psi_f^{\mathcal{R}}(E,R,t)|^2. \tag{7}$$

After summation of these partial intensities over all regions $\mathcal{R}$ we obtain spectra in which interferences occurring between neighboring regions are suppressed. By comparing with the total Auger spectrum $\sigma_f(E)$ one can easily identify these interferences. When subdividing the position space into, for instance, two regions and then shifting the line of division R_t gradually, an analysis of the origin of the different contributions is made possible.

In Fig. 12 this method is applied to the ''three-peak'' spectrum obtained at an excitation energy of 689 eV. Here, we have divided the whole space into two regions at the internuclear distance R_t, and then shifted R_t successively towards larger internuclear distances from top to bottom and from left to right in the figure. The ''spatially resolved'' partial intensities $\sigma_f^{\mathcal{R}}(E)$ are always shown reflected at the x axis in dashed and solid lines. Above the axis, their sum $\Sigma_{\mathcal{R}}\sigma_f^{\mathcal{R}}(E)$ (thick line) is depicted and compared to the exact Auger spectrum $\sigma_f(E)$ (thin line). A mismatch between

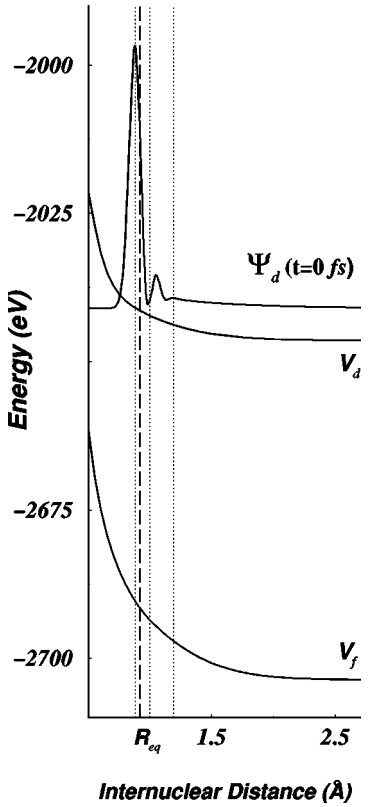

FIG. 11. Potential curves of the core-excited $^1\Sigma$ state and the cationic $^4\Pi$ final state shown together with the intermediate-state wave packet Ψ_d at $t=0$, the center of the excitation pulse, for an excitation energy of 689 eV. The dashed line shows the equilibrium distance of HF ($R_{eq}=0.92$ Å). The dotted lines indicate the division into different spatial regions $\mathcal{R}$. The space is divided at the internuclear distances $R_t=0.88$ Å, 1 Å, and 1.19 Å. The corresponding partial intensities $\sigma_f^{\mathcal{R}}(E)$ are shown in the first three frames of Fig. 12.

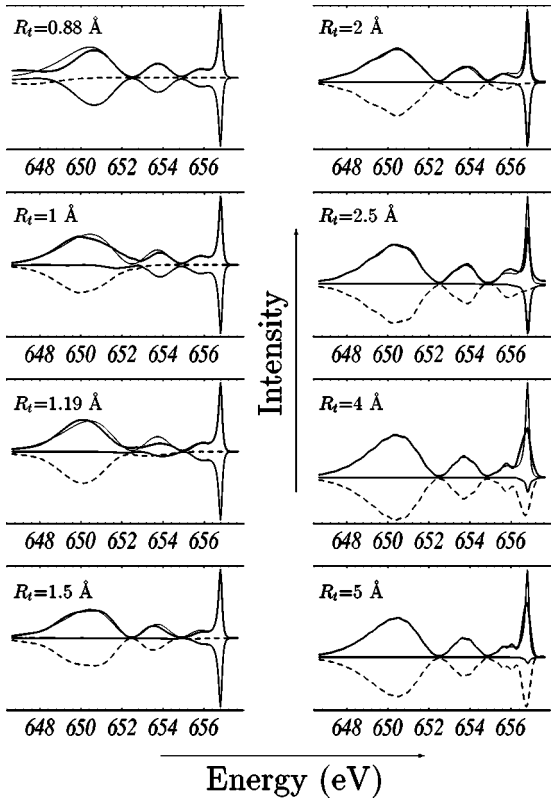

FIG. 12. Comparison of the total spectrum $\sigma_f(E)$ (thin line) of Fig. 3 (obtained at an excitation energy of 689 eV) with the two ''spatially resolved'' partial intensities $\sigma_f^{\mathcal{R}}(E)$ (displayed reflected at the x axis in thin and dashed lines) as defined in Eq. (7) and their sum $\Sigma_{\mathcal{R}}\sigma_f^{\mathcal{R}}(E)$ (thick line). The two partial contributions originate from the regions $\mathcal{R}$ of internuclear distance above and below a dividing value R_t, which increases from top to bottom and from left to right.

these graphs indicates the importance of interference in the final state between the two spatial regions of decay, because these interferences are suppressed in $\Sigma_{\mathcal{R}}\sigma_f^{\mathcal{R}}(E)$. One immediately notices that the parts of the spectrum, which are affected by the suppression of interference between neighboring regions, shift from lower to higher Auger energies with increasing R_t. For a subdivision at small internuclear distances, only the molecular part of the spectrum is affected and can thus be assigned to transitions in a region between 0.8 and 2 Å. The formation of the atomic peak begins at internuclear distances of about 2 Å and is nearly complete when the atomic fragments are separated by about 5 Å.

Let us now turn to a more detailed analysis of the ''mapping'' effect, i.e., the question of the extent to which the simple picture of assigning an internuclear region to a spectral region is valid. We find the following: The first peak of the spectrum at about 651 eV is clearly formed at internuclear distances between 0.88 and 1 Å (see Fig. 12, first and second frame). In accordance with the expected mapping it can thus be ascribed to transitions coming from the first peak in the intermediate-state wave packet (see Fig. 11). The second spectral peak can be assigned to an internuclear region between 1 and 1.5 Å. This stands already in contrast to the simple mapping picture: The peak lies clearly in the molecular region but is formed by transitions in an internuclear region where the second as well as the third peak of the intermediate-state wave packet are found (see Fig. 11). The third spectral peak is finally only formed for relatively large internuclear distances (>1.5 Å) where the intermediate-state wave packet is already smooth. Interference-causing contributions to this peak still occur at internuclear distances where already the atomic peak is being formed. We can thus conclude that a simple mapping is only valid for intense and long-lived spectral structures. For the weaker contributions, coming later in time and from transitions at larger internuclear distances, however, long-range interferences (i.e., interactions between contributions resulting from transitions at very different spatial regions) take place in the final-state wave packet and become responsible for the structures found in the spectrum. Why, nevertheless, such a simple three-peak structure mimicking the structure of the intermediate-state wave packet appears in the present spectrum, remains an open question.

V. CONCLUSIONS

In this contribution we have analyzed the impact of an energetically selective excitation on decay spectra resulting from transitions between purely dissociative states. Due to the comparable time scales of excitation and internal motion of the core-excited molecule, interferences can take place

and shape the intermediate-state wave packet $\Psi_d(t)$. We have seen that the impact of interferences on the observed spectra is weaker when excitation takes place at the resonance energy or below it than when detuning above the resonance. While the on-resonance spectrum closely resembles the Auger spectrum after broad-band excitation, with its typical two-peak structure formed by the molecular and atomic contributions, detuning the excitation energy slightly above the resonance leads to a very pronounced interference structure in the molecular part of the spectrum. For stronger detuning the decay spectra are formed during the excitation process, before the nuclear wave packets have much time to propagate. This leads to a quenching of the atomic peak and to a general suppression of interferences.

In order to study the impact of detuning, we have focused on one special contribution to the resonant Auger spectrum of HF originating from a transition between two purely repulsive potential curves. The example of HF is very well suited for this study because the lowest-lying core-excited state is very well separated from the higher-lying Rydberg states, which allows for large detuning (up to almost 4 eV) without opening competitive channels. Apart from this fact, similar effects are always expected for transitions from a dissociative intermediate state as soon as the energy width of the excitation pulse becomes comparable to the decay width.

The mechanisms of interference have been very clearly revealed by studying the time evolution of the intermediate-state wave packet $\Psi_d(R,t)$ and the Auger spectrum $\sigma_f(E)$ thoroughly. Besides the comparability of the underlying time scales, we have shown that the extent of interference depends crucially on the spatial confinement of parts of the decaying wave packet in the zone of its creation (about the equilibrium distance of the initial electronic state). When exciting at the resonance or below it, the created wave packet $\Psi_d(R,t)$ immediately experiences the repulsive forces of the dissociative potential to which it was transferred and leaves the zone of its creation very quickly. Interference is thus suppressed. When exciting at higher excitation energies, on the contrary, parts of the created wave packet $\Psi_d(R,t)$ can now propagate towards smaller internuclear distances. Additionally, the creation zone is enlarged because also shorter internuclear distances are accessible by the above-resonance excitation. Thus, parts of $\Psi_d(R,t)$ can now remain longer in the interaction zone and interferences become more pronounced. This leads to the desired energy selection and to the development of a nodal structure in $\Psi_d(R,t)$ corresponding to the nodal structure of the eigenvectors in the selected region. This structure is then mapped onto the Auger spectrum owing to the dissociative nature of the final-state potential curve: Transitions occurring at large internuclear distances contribute at higher Auger energies than those at smaller distances. Nevertheless, this simple picture of a ''direct mapping'' of structures found in the intermediate-state wave packet onto the Auger spectrum applies only for strong and long-lived structures at small internuclear distances. For the less-intense parts, long-range interference (i.e., interference between contributions coming from transitions at very different internuclear distances) in the final-state wave packet becomes important and may influence the spectrum—the simple mapping picture is not valid.

For the detailed analysis of this mapping we have presented a method, based on the wave-packet approach, which allows us to analyze and identify the regions of internuclear distance responsible for different contributions of decay spectra. This analysis also enables us, in general, to answer the question about the internuclear distances from which one can speak of ''atomic'' transitions.

Especially in this paper, the time-dependent wave-packet propagation has clearly proven its advantages over the traditional time-independent approach. By making accessible the time resolution of the physically relevant quantities one obtains insight into the underlying interference mechanisms, which are otherwise difficult to understand.

ACKNOWLEDGMENT

Financial support by the Deutsche Forschungsgemeinschaft (DFG) is gratefully acknowledged.

[1] E. Pahl, L. S. Cederbaum, H.-D. Meyer, and F. Tarantelli, Phys. Rev. Lett. **80**, 1865 (1998).

[2] M. Neeb, J.-E. Rubensson, M. Biermann, and W. Eberhardt, J. Electron Spectrosc. Relat. Phenom. **67**, 261 (1994).

[3] M. Neeb, J.-E. Rubensson, M. Biermann, W. Eberhardt, K. J. Randall, J. Feldhaus, A. L. D. Kilcoyne, A. M. Bradshaw, Z. Xu, P. D. Johnson, and Y. Ma, Chem. Phys. Lett. **212**, 205 (1993).

[4] M. N. Piancastelli, M. Neeb, A. Kivimäki, B. Kempgens, H. M. Köppe, K. Maier, and A. M. Bradshaw, Phys. Rev. Lett. **77**, 4302 (1996), and refernces therein.

[5] E. Kukk, A. Wills, N. Berrah, B. Langer, J. D. Bozek, O. Nayadin, M. Alsherhi, A. Farhat, and D. Cubaynes, Phys. Rev. A **57**, R1485 (1998).

[6] P. Skytt, J. Guo, N. Wasdahl, J. Nordgren, Y. Luo, and H. Ågren, Phys. Rev. A **52**, 3572 (1995).

[7] P. Glans, K. Gunnelin, P. Skytt, J.-H. Guo, N. Wassdahl, J. Nordgren, H. Ågren, F. K. Gel'mukhanov, T. Warwick, and E. Rotenberg, Phys. Rev. Lett. **76**, 2448 (1996).

[8] L. S. Cederbaum and F. Tarantelli, J. Chem. Phys. **98**, 9691 (1993).

[9] L. S. Cederbaum and F. Tarantelli, J. Chem. Phys. **99**, 5871 (1993).

[10] E. Pahl, H.-D. Meyer, and L. S. Cederbaum, Z. Phys. D **38**, 215 (1996).

[11] E. Pahl, H.-D. Meyer, L. S. Cederbaum, D. Minelli, and F. Tarantelli, J. Chem. Phys. **105**, 9175 (1996).

[12] F. Gel'mukhanov, L. Mazalov, and A. Kondratenko, Chem. Phys. Lett. **46**, 133 (1977).

[13] F. Kaspar, W. Domcke, and L. S. Cederbaum, Chem. Phys. **44**, 33 (1979).

[14] N. Correia, A. Flores-Riveros, H. Ågren, K. Helenelund, L. Asplund, and U. Gelius, J. Chem. Phys. **83**, 2035 (1985).

[15] A. Cesar, H. Ågren, and V. Carravetta, Phys. Rev. A **40**, 187 (1989).

[16] E. Pahl, L. S. Cederbaum, and F. Tarantelli, Phys. Rev. A **60**, 1070 (1999).
[17] T. J. Park and J. C. Light, J. Chem. Phys. **85**, 5870 (1986).
[18] C. Leforestier, R. H. Bisseling, C. Cerjan, M. D. Feit, R. Friesner, A. Guldberg, A. Hammerich, G. Jolicard, W. Karrlein, H.-D. Meyer, N. Lipkin, O. Roncero, and R. Kosloff, J. Comput. Phys. **94**, 59 (1991).
[19] U. Manthe, H. Köppel, and L. S. Cederbaum, J. Chem. Phys. **95**, 1708 (1991).
[20] D. T. Colbert and W. H. Miller, J. Chem. Phys. **96**, 1982 (1992).
[21] A. P. Hitchcock and C. Brion, J. Phys. B **14**, 4399 (1981).
[22] S. Svensson, L. Karlsson, N. Mårtensson, P. Baltzer, and B. Wannberg, J. Electron Spectrosc. Relat. Phenom. **50**, c1 (1990).
[23] K. Faegry, Jr. and H. P. Kelly, Phys. Rev. A **19**, 1649 (1979).
[24] K. Zähringer, H.-D. Meyer, and L. S. Cederbaum, Phys. Rev. A **45**, 318 (1992).
[25] O. Björnelholm, S. Sundin, S. Svensson, R. R. T. Marinho, A. Naves de Brito, F. Gel'mukhanov, and H. Ågren, Phys. Rev. Lett. **79**, 3150 (1997).
[26] F. Gel'mukhanov and H. Ågren, Phys. Rev. A **54**, 379 (1996).
[27] G. S. Brown, M. H. Chen, B. Crasemann, and G. E. Ice, Phys. Rev. Lett. **45**, 1937 (1980).
[28] J. Jauhiainen, H. Aksela, O.-P. Sairanen, E. Nommiste, and S. Aksela, J. Phys. B **56**, R3345 (1996).
[29] Z. F. Liu, G. B. Bancroft, K. H. Tan, and M. Schachter, Phys. Rev. Lett. **72**, 621 (1993).
[30] Y. F. Hu, G. M. Bancroft, J. Karvonen, E. Nommiste, A. Kivimaki, H. Aksela, S. Aksela, and Z. F. Liu, Phys. Rev. A **56**, R3342 (1997).